ACSNANO
www.acsnano.org
ARTICLE

# Reverse Microemulsion Synthesis of Sulfur/Graphene Composite for Lithium/Sulfur Batteries

Mohammad Rejaul Kaiser,[†,‡] Zhaohui Ma,[†] Xiwen Wang,[†] Fudong Han,[†] Tao Gao,[†] Xiulin Fan,[†] Jia-Zhao Wang,[‡] Hua Kun Liu,[‡] Shixue Dou,[‡] and Chunsheng Wang*[,†]

[†]Department of Chemical and Biomolecular Engineering, University of Maryland, College Park, Maryland 20742, United States
[‡]Institute for Superconducting and Electronic Materials, University of Wollongong, Wollongong, NSW 2522, Australia

Supporting Information

**ABSTRACT:** Due to its high theoretical capacity, high energy density, and easy availability, the lithium−sulfur (Li−S) system is considered to be the most promising candidate for electric and hybrid electric vehicle applications. Sulfur/carbon cathode in Li−S batteries still suffers, however, from low Coulombic efficiency and poor cycle life when sulfur loading and the ratio of sulfur to carbon are high. Here, we address these challenges by fabricating a sulfur/carboxylated−graphene composite using a reverse (water-in-oil) microemulsion technique. The fabricated sulfur−graphene composite cathode, which contains only 6 wt % graphene, can dramatically improve the cycling stability as well as provide high capacity. The electrochemical performance of the sulfur−graphene composite is further enhanced after loading into a three-dimensional heteroatom-doped (boron and nitrogen) carbon-cloth current collector. Even at high sulfur loading (~8 mg/cm$^2$) on carbon cloth, this composite showed 1256 mAh/g discharge capacity with more than 99% capacity retention after 200 cycles.

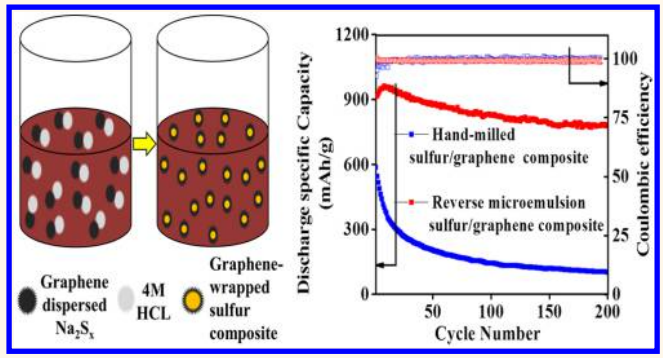


**KEYWORDS:** *reverse microemulsion, surfactants, sulfur solubility, carboxylated graphene, functionalized carbon cloth, sulfur cathode*

Li-ion batteries have been dominant over other battery systems for portable devices (*e.g.*, smart phones, laptop computers, cameras, *etc.*), but they barely can meet the energy and power requirements for electric and hybrid electric vehicles.[1] The current Li-ion batteries can deliver gravimetric energy density of 160−190 Wh/kg, which can, at most, run an electric vehicle for 150 to 200 km. The main hurdle for low energy density Li-ion batteries comes from their transition metal oxide cathodes, which can only deliver a theoretical capacity of 150−170 mAh/g.[2]

Sulfur, which exhibits 2600 Wh·kg$^{-1}$ specific energy when coupled with lithium, is inexpensive, naturally abundant, and environmentally benign, so it could be a better and more promising alternative to the existing transition metal oxide cathode materials. Even though the Li/S system has been under investigation for the last 30 years, it is yet to be commercialized[3] due to three main challenges: (i) the very low electrical and ionic conductivities of sulfur, leading to limited active material utilization; (ii) dissolution into the electrolyte of long-chain polysulfides and the polysulfide shuttle, which causes low cycling stability; and (iii) volume changes in the active material during charge and discharge, which causes degradation of the cathode. Extensive research has been conducted on loading sulfur onto different conductive carbon materials,[4−8] in combination with different electrolytes,[9,10] binders,[11,12] and additives.[13−17] In most cases, a high initial capacity (>1000 mAh/g) was achieved, but the capacity still gradually decays with charge/discharge cycling.

Graphene, along with its derivatives (reduced graphene, functionalized graphene, heteroatom-doped graphene, *etc.*), has high electronic conductivity and high surface area and is considered one of the most promising carbons to ameliorate the challenges of the Li/S system.[18−20] Considerable research has been conducted on graphene/sulfur composites to increase the capacity and stability of the Li/S system. In most cases, however, the graphene/sulfur composites were fabricated either by mechanical milling or by chemical precipitation methods,[19,21,22] where the graphene was not exfoliated or firmly

Received: May 23, 2017
Accepted: August 29, 2017
Published: August 29, 2017




DOI: 10.1021/acsnano.7b03591
*ACS Nano* 2017, 11, 9048−9056

Table 1. Solubility of Sulfur in Common Organic Solvents[29]

| solvent | solubility (wt %) | solvent | solubility (wt %) | solvent | solubility (wt %) | solvent | solubility (wt %) |
|---|---|---|---|---|---|---|---|
| ethanol | 0.066 | *n*-hexane | 0.400 | acetone | 0.079 | aniline | 1.259 |
| carbon tetrachloride | 0.832 | xylene | 2.051 | nitrobenzene | 0.856 | diethyl ether | 0.181 |
| cyclohexane | 1.185 | toluene | 2.070 | chloroform | 1.164 | chlorobenzene | 2.370 |
| benzene | 2.093 | carbon disulfide | 34.800 | diethylformamide | 0.191 | bromoform | 3.640 |

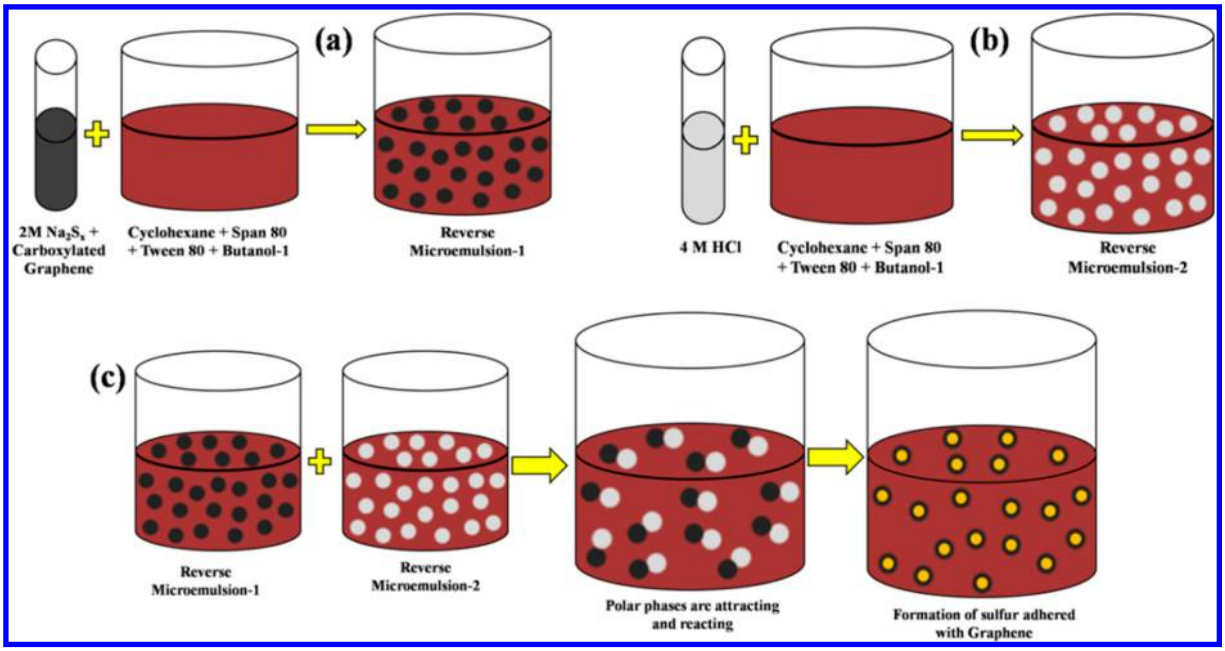


Figure 1. Schematic illustration of the reverse microemulsion method: (a) preparing microemulsion-1, (b) preparing microemulsion-2, and (c) synthesis of sulfur/graphene composite.

adhered to the sulfur, thus requiring a high ratio of graphene to sulfur to physically separate the sulfur from the liquid electrolyte. To improve the cycling performance and stability, it is important to have better adhesion between the sulfur/sulfide and the graphene, and they need to be uniformly mixed each other with a high sulfur loading, which will not only help the overall capacity but also maintain the structural integrity during expansion and contraction of the sulfur. It is hard, however, to synthesize such a graphene/sulfur nanocomposite using traditional technologies.

The water-in-oil microemulsion (w/o microemulsion) or reverse microemulsion method, commonly used for the synthesis of uniform composite nanoparticles from their salt solutions,[23,24] can be used for the synthesis of graphene/sulfur nanoparticles with strong adhesion in the sulfur/sulfide carboxyl-functionalized graphene. In the w/o microemulsion or reverse microemulsion method, an aqueous solution containing metal salts is dispersed in an organic oil phase with the help of a surfactant, and this microemulsion is designated as microemulsion-1, whereas another microemulsion (designated as microemulsion-2) is prepared, in which an aqueous solution containing a reducing agent is dispersed in the same organic oil phase. Then, these two emulsions are mixed together, and the aqueous phases merge and react with each other to form metal or composite nanoparticles.[24] Microemulsions have been used by the scientific community for the last 60 years in different fields,[25−27] but they are yet to be used for the synthesis of sulfur/carbon composites. This is because the synthesized sulfur from the reverse microemulsion method is a nonpolar molecule and dissolves in almost all the organic nonpolar solvents that generally have been used as the oil phase in the reverse microemulsion method. Herein, we used sulfur-dissolved saturated cyclohexane (sulfur solubility of 1.185 wt %) as the oil phase, so that the synthesized sulfur could not dissolve in the cyclohexane. We synthesized our sulfur/graphene composite with a 94% S ratio by mixing two emulsions to form graphene-coated/adhered sulfur, in which microemulsion-1 was synthesized by adding an aqueous carboxylated graphene−sodium polysulfide suspension solution into cyclohexane oil while microemulsion-2 was synthesized by adding an aqueous solution of hydrochloric acid into cyclohexane. With an electrode consisting of the S/C composite on a three-dimensional (3-D) heteroatom-doped carbon-cloth current collector (loading of active materials 8 mg/cm$^2$), 1256 mAh/g discharge capacity was obtained with more than 99% capacity retention after 200 cycles.

## RESULTS AND DISCUSSION

**Reverse Microemulsion and Selection of Materials.** A dispersion consisting of water, oil, and surfactant(s) is an isotropic and thermodynamically stable system. A dispersion with a domain diameter of ∼1 to 100 nm is called a microemulsion. If the dispersed phase is water or an aqueous solution and the continuous phase is an organic liquid (an "oil"), it is called a water-in-oil (w/o) microemulsion or reverse microemulsion.[28] In our method, 2 M $Na_2S_x$ solution mixed with carboxylated graphene was used as the aqueous phase. The carboxylated graphene can form hydrogen bonds with water, which helps to uniformly disperse the graphene in the water, whereas $Na_2S_x$ can reacts with HCl to form hydrogen sulfide



DOI: 10.1021/acsnano.7b03591
ACS Nano 2017, 11, 9048−9056

($H_2S$) and sodium chloride (NaCl), where the $H_2S$ gas cannot affect the ratio of aqueous phase to oil phase. $Na_2S_2O_3$, which is low-cost, widely available, and generally used to synthesize the sulfur chemically, produces $H_2O$ as a byproduct. This extra water will cause an imbalance in the ratio of aqueous phase to oil phase, and hence, $Na_2S_2O_3$ has been avoided in our work.

The oil phase must be nonpolar, hydrophobic, and feature extremely low solubility of sulfur. In addition, the oil must have very good compatibility with the surfactant and cosurfactant to produce a uniform microemulsion. No organic oil can fulfill all these requirements. Table 1 shows the solubility limits of sulfur in common organic solvents, and the left column shows the solubility of sulfur in nonpolar solvents apart from ethanol. Among them, carbon tetrachloride and *n*-hexane show low solubility of sulfur, but they cannot form a stable and uniform microemulsion. Cyclohexane, which has 1.185 wt % solubility of sulfur, can form an extremely stable and uniform microemulsion with sorbitan mono-oleate (Span 80) and polyethylene glycol (PEG-20) sorbitan mono-oleate (Tween 80) surfactants.[30] These two surfactants have very low surface tension, with a hydrophilic−lipophilic balance (HLB) of 4.3 and 15, respectively. A lower HLB number indicates higher hydrophobicity and *vice versa*. In the reverse microemulsion method, a large amount of oil and small amount of water are generally used, and because of that, a ratio of 8:1 of Span 80 and Tween 80 surfactants was used in 450 mL of cyclohexane. Moreover, it was found that, to form a stable reverse microemulsion, the HLB of the surfactant should be in the range of 3 to 6.[31] Figure 1 presents a schematic illustration of the preparation of the reverse microemulsions and the synthesis of the sulfur−graphene composite from these emulsions, where the cyclohexane was saturated with sulfur before it was used as an oil phase. Photographs of the products in the reverse microemulsion method and synthesis of the sulfur−graphene composite are shown in Figure S1 in the Supporting Information.

The nanosized sulfur synthesized using the reverse microemulsion method has better adhesion to carboxylated graphene, improving the electronic conductivity and utilization of the sulfur in the electrode. Moreover, carboxyl functional groups on graphene can attract polysulfides, thus reducing the polysulfide shuttle reactions. The graphene content in our sulfur/graphene composite is 6.1 wt %, which was measured by thermogravimetric analysis (TGA) (Figure S2). The conductivity of the synthesized composite, along with those of carboxylated graphene, commercial sulfur, and hand-mixed sulfur−graphene composite with the same weight percent of graphene, was measured with a four probe Signatone conductivity tester, and the results are shown in Table 2.

As shown in Table 2, the conductivity of the RM-S/G composite is 2 orders of magnitude higher than that of the hand-mixed sulfur−graphene composite with the same composition. The increased conductivity of RM-S/G is due to better adhesion and exfoliation of graphene in the sulfur and the uniform distribution of sulfur on graphene. The particle size and morphology of the synthesized RM-S/G were characterized using scanning electron microscopy (SEM). As shown in Figure 2a,b, the graphene firmly adheres to the sulfur, forming 10 to 20 $\mu$m S/G composite particles. It has been reported that the cyclohexane, Span 80, and Tween 80 system is one of the most stable microemulsions with uniform micelle size.[30] The size of the micelles synthesized using Span 80 and Tween 80 in cyclohexane oil is approximately 7 to 100 nm,[30] which is much smaller than the sizes of the S/G composite particles. It is possible that 10 to 20 $\mu$m sulfur particles are induced by agglomeration of nanoscale sulfur during the nucleation and growth. Figure 2c,d shows transmission electron microscope (TEM) micrographs of the RM-S/G composite. It is clear that the crystalline graphene sheets, which have a moiré pattern, are exfoliated and well-distributed inside the sulfur particles. The graphene that is trapped inside the big sulfur particles demonstrates that the sulfur particles are agglomerated from graphene-coated sulfur nanoparticles during the nucleation and growth process.

To further confirm the entrapment of graphene inside the sulfur, a sample of microsized sulfur/graphene composite was ball-milled (in the presence of isopropyl alcohol at 300 rpm), so that all the graphene sheets that were entrapped inside the sulfur particles could be exposed. The SEM micrograph of RM-S/G composite in Figure 2e shows the morphology of the sulfur/graphene composite after the ball milling, where smaller sized sulfur/graphene composite particles are observed. Each smaller particle contains carboxylated graphene sheets adhering to the sulfur particles that have been exposed after ball milling. It can be deduced from this that the large particles shown in Figure 2b are mainly composed of smaller sized sulfur/graphene composite particles.

The phase structure of the RM-S/G composite along with that of graphene was characterized using X-ray diffraction (XRD, Figure 3a). Along with other small peaks, RM-S/G exhibits a characteristic peak of crystalline octa-sulfur ($S_8$) at around 23.1° that is diffracted from the (222) planes. This characteristic peak at 23.1° is broadened for the RM-S/G composite compared to commercial sulfur, which indicates the smaller particle size of sulfur. Nevertheless, no significant peak broadening occurs after the ball milling of the RM-S/G composite, which means that the crystallite size remains same and that the disparity of particle sizes is due to the physical adhesion of micro- and nanosized particles. The Raman spectra of pure sulfur and RM-S/G composite are presented in Figure 3b, and all the spectra show sharp peaks at 219.1 and 473.2 $cm^{-1}$, which reflect the bending and the stretching of nonpolar S−S bonds, respectively.[32] Moreover, the RM-S/G composite shows small peaks around 1400 and 1600 $cm^{-1}$, which are the characteristic peaks of the D band and the G band for carbon, respectively.[33] The D and G bands of the RM-S/G composite are very weak, confirming that graphene is buried inside the RM-S/G due to the aggregation of graphene-coated nanosulfur particles. After ball milling, the graphene sheets are exposed to the laser radiation and exhibit higher intensity of the D and G bands of carbon in the ball-milled RM-S/G. Due to the confinement and exfoliation of graphene inside the sulfur particles, electrons not only can strike the surface of the sulfur/graphene composite but also can pass through the RM-S/G particles, and thus, the RM-S/G composite shows higher conductivity compared to that of the hand-mixed sulfur−

**Table 2. Electronic Conductivity of Sulfur-Based Materials**

| sample | conductivity (S/cm) | sample | conductivity (S/cm) |
|---|---|---|---|
| pure sulfur | $3.32 \times 10^{-25}$ | reverse microemulsion sulfur−graphene (RM-S/G) composite | $7.92 \times 10^{4}$ |
| carboxylated graphene | $4.09 \times 10^{6}$ | hand-mixed sulfur−graphene composite | $3.27 \times 10^{2}$ |



DOI: 10.1021/acsnano.7b03591
ACS Nano 2017, 11, 9048−9056

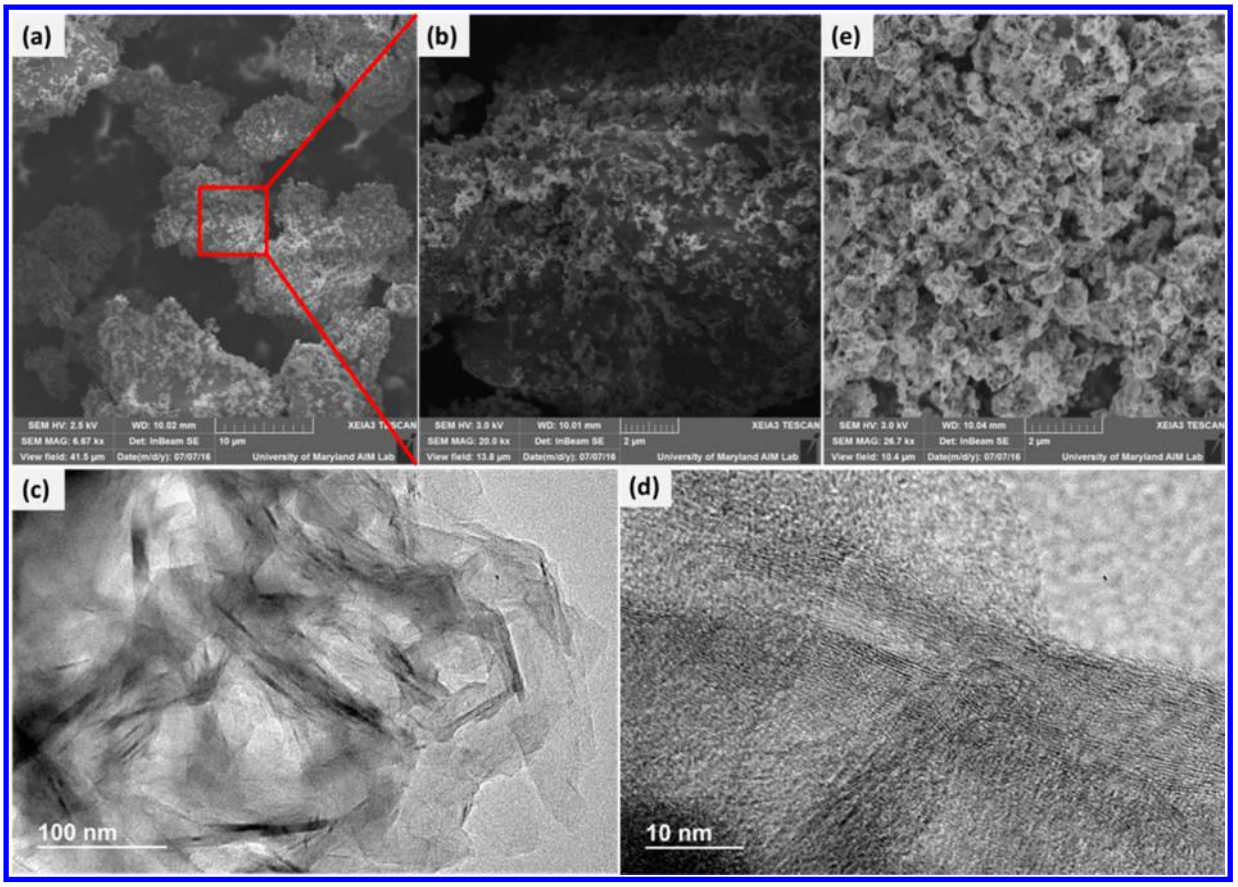


Figure 2. SEM and TEM micrographs of RM-S/G: (a,b) SEM images of the as-synthesized composite at different magnifications; (c,d) TEM micrographs that prove the presence and exfoliation of graphene inside the sulfur; and (e) SEM image of ball-milled RM-S/G composite.

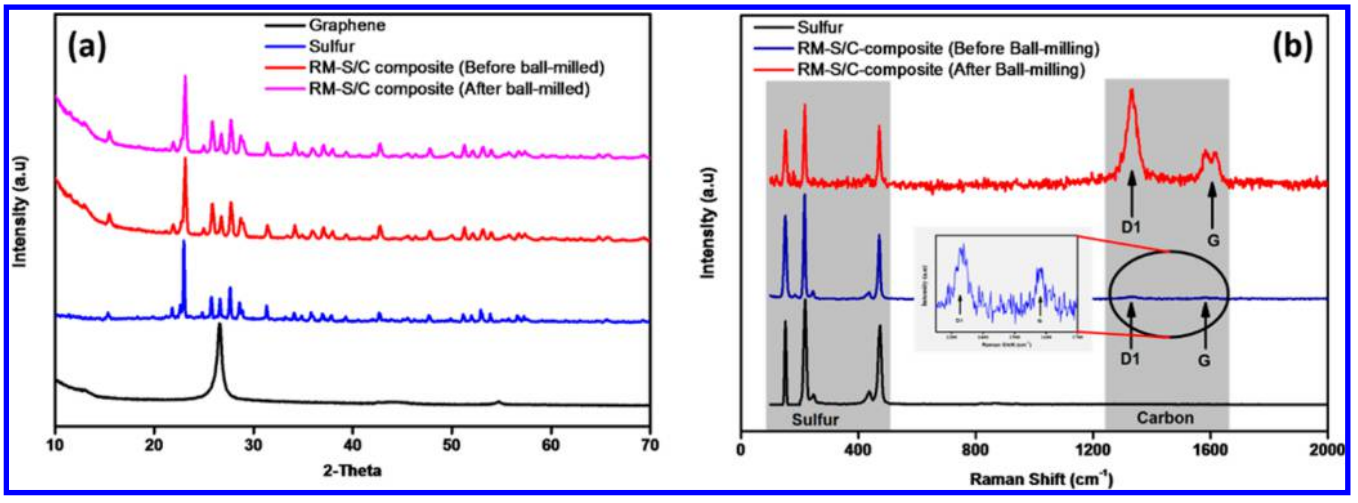


Figure 3. XRD patterns (a) and Raman spectra (b) of the RM-S/G composite before and after ball milling.

graphene composite, where the graphene only adheres to the surfaces of the sulfur particles.

The presence of carboxyl groups in both graphene and the RM-S/G composite was confirmed by Fourier transform infrared (FTIR) spectroscopy. Figure S3 shows the FTIR spectra of graphene, RM-S/G composite, and sulfur. It is shown that both graphene and the RM-S/G composite feature two sharp peaks at 1760 and 2890 $cm^{-1}$, which are characteristic peaks of C═O stretching and O−H stretching for carboxyl groups, whereas no characteristic peaks of C═O stretching and O−H stretching exist in the sulfur sample. The very sharp peak that appears at 2400 $cm^{-1}$ in sulfur is attributed to the symmetric stretching of water ($H_2O$) that comes from moisture. It is important to note here that the intensity of the O−H stretching peak is decreased after the formation of the RM-S/G composite and that the peak intensity decreases even further after ball milling. The breakage of hydrogen bonds is responsible for this. The lower the amount of hydrogen bond formation, the lower the intensity of the O−H stretching peak will be. These carboxyl groups play a pivotal role in the exfoliation and the uniform dispersion of graphene in aqueous solution, as well as the bonding of lithium polysulfide onto



DOI: 10.1021/acsnano.7b03591
ACS Nano 2017, 11, 9048−9056

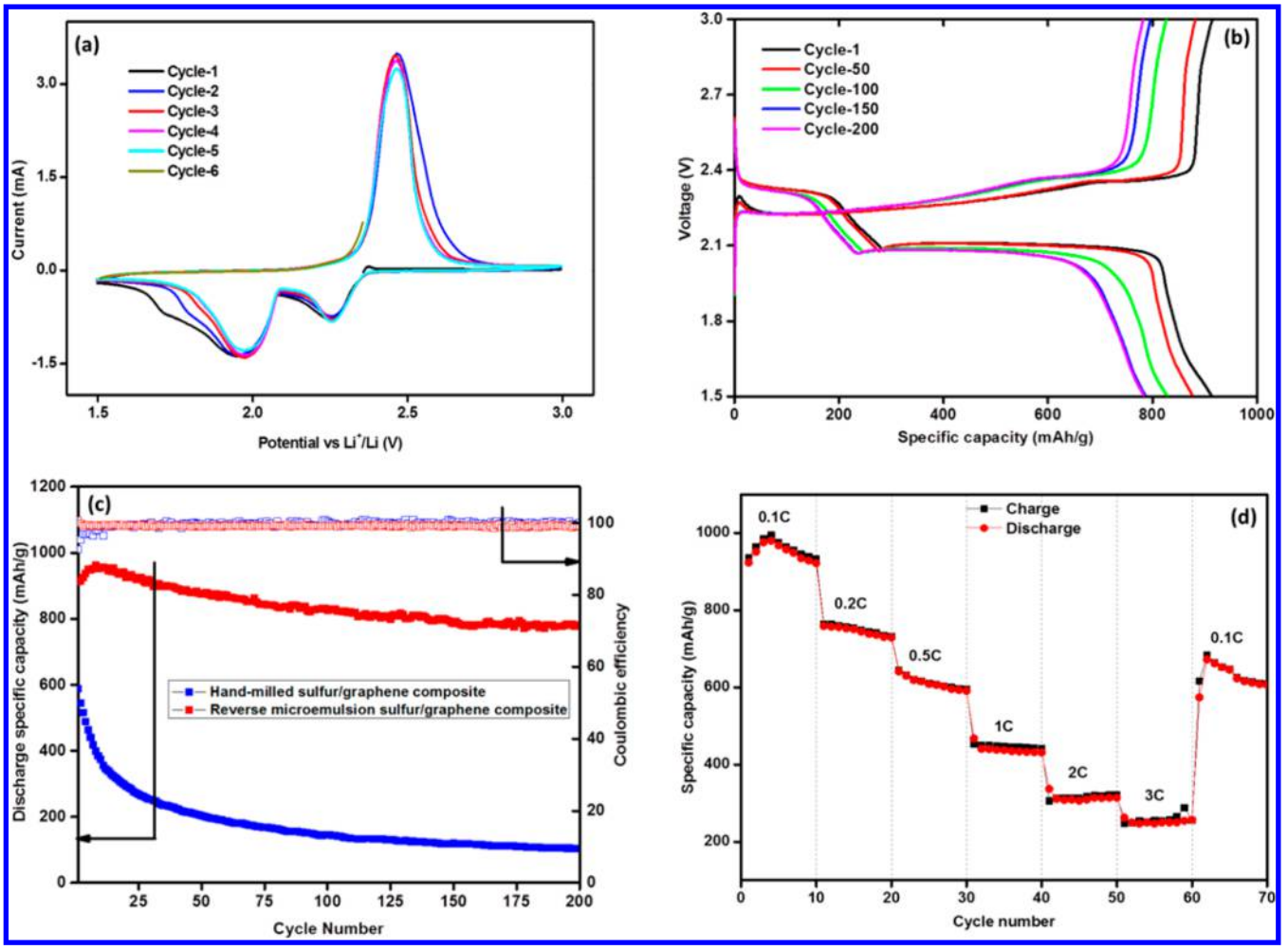


**Figure 4. Electrochemical performance for low loading (1−2 mg/cm$^2$) of the RM-S/G composite on Al current collector: (a) cyclic voltammograms of the RM-S/G composite for the first 6 cycles at a scan rate of 0.1 mV s$^{-1}$; (b) galvanostatic charge−discharge curves for selected cycles of the RM-S/G composite at 0.1 C; (c) cycling performance of the RM-S/G composite and hand-milled sulfur/graphene composite at a current density of 0.1 C; and (d) rate capability of the RM-S/G composite at different current densities.**

graphene to stabilize the capacity during charge/discharge cycling.

**Electrochemical Performance of the RM-S/G Composite.** The electrochemical performance of the RM-S/G composite was evaluated by both cyclic voltammetry and galvanostatic charge−discharge cycling. The cyclic voltammograms (CVs) of the RM-S/G composite in Figure 4a show two reduction peaks and one oxidation peak, with a small deviation in intensity with increasing cycle number. The first reduction peak appearing at 2.3−2.4 V is related to the change from elemental sulfur to long-chain lithium polysulfides ($Li_2S_n$, $n \geq 4$), and the second reduction peak appearing at 1.9−2.0 V reflects the reduction of long chain lithium polysulfides to short chain lithium polysulfides ($Li_2S_n$, $n < 4$), which is in agreement with the two plateaus of the RM-S/G composite in the galvanostatic charge/discharge profiles in Figure 4b.[34] In the charging profile, a small bump is observed at 2.3 V, which later disappears with cycling, the position of which resembles the activation energy of polysulfide formation from $Li_2S$. For the first cycle, the energy barrier is quite high, but in the following cycles, it is reduced significantly due to the presence of polysulfides that were formed in the previous cycle. It is well-established that the presence of trace amounts of polysulfides significantly reduces the activation barrier of $Li_2S$.[35,36] It is important to note here that the reduction peak represented by a small bump at 1.7 V in the first two cycles of CVs is due to the reduction of $LiNO_3$ salt, which can help to form a stable solid electrolyte interphase on the lithium metal surface,[37] thus reducing the shuttle reaction. The cycling behaviors of the RM-S/G composite and hand-milled sulfur/graphene composite at a current density of 0.1 C are shown in Figure 4c. Both the hand-milled sulfur−graphene composite and the RM-S/G composite cathodes consist of 6 wt % graphene, 34 wt % carbon black, 50 wt % sulfur, and 10 wt % poly(vinylidene fluoride) (PVDF). On the other hand, commercial sulfur contains no graphene, but the sulfur content remains the same (~50 wt %). All three sulfur cathodes show typical charge/discharge behavior with two plateaus at 2.4 and 2.1 V. The RM-S/G composite, however, shows much higher capacity and cycling stability than the hand-milled sulfur/graphene composite. The hand-milled sulfur/graphene composite cathode shows an initial discharge capacity of 587 mAh/g (based on sulfur), which drops to 103 mAh/g after 200 cycles, representing 17.5% of the initial capacity. The RM-S/G composite shows a much higher initial discharge capacity of 914 mAh/g (based on sulfur) and retains discharge capacity of 731 mAh/g after 200 cycles. The capacity retention of the RM-S/G composite (around 80%) is 62% higher than that of the



DOI: 10.1021/acsnano.7b03591
ACS Nano 2017, 11, 9048−9056

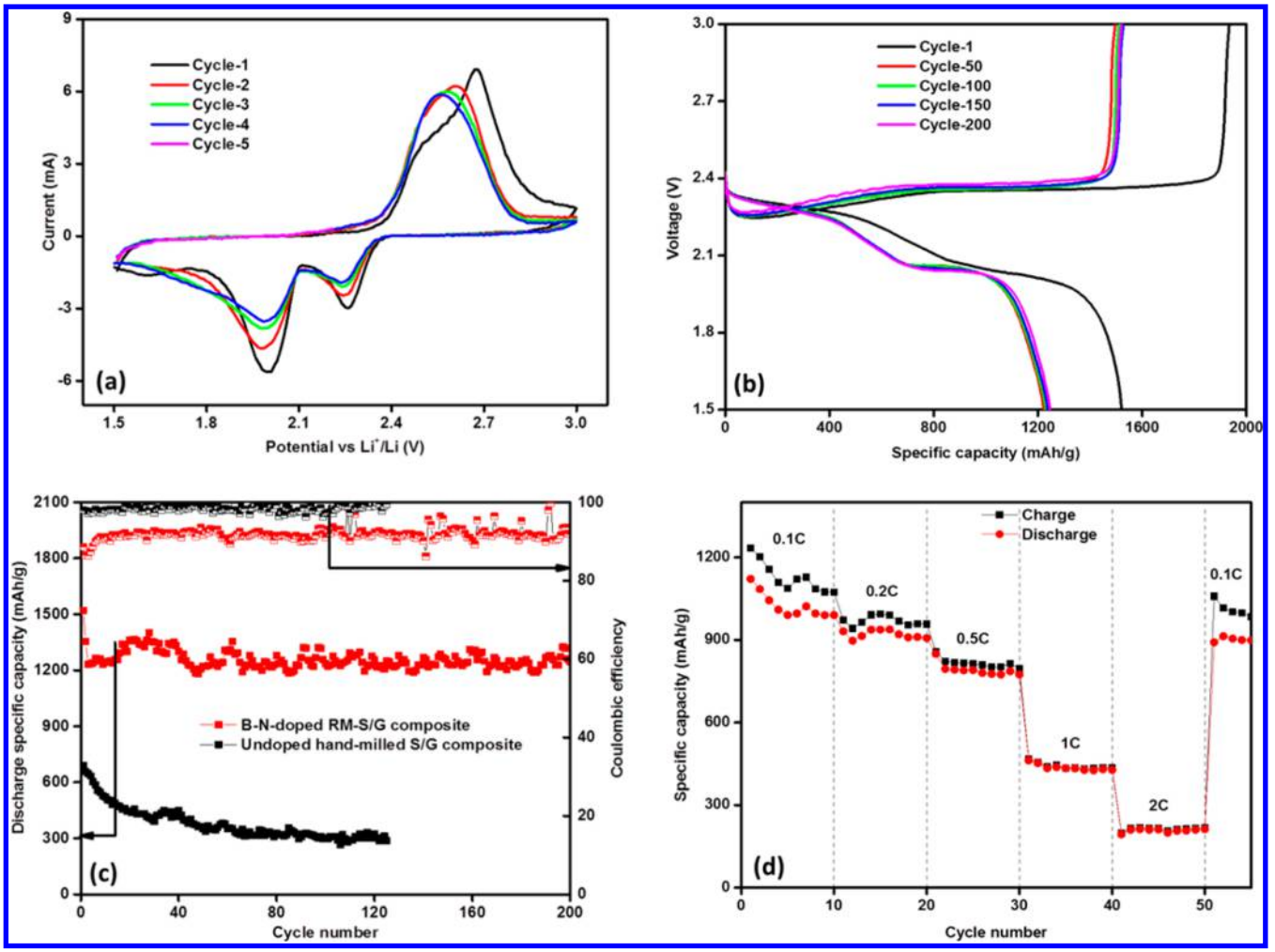


**Figure 5. Electrochemical performance of the RM-S/G composite loaded on boron, nitrogen-doped carbon cloth: (a) cyclic voltammograms for the first 5 cycles of doped RM-S/G composite at a scan rate of 0.1 mV $s^{-1}$; (b) galvanostatic charge−discharge curves for selected cycles of doped RM-S/G composite at 0.1 C; (c) cycling performance of B,N-doped RM-S/G composite and hand-milled undoped sulfur/graphene in functionalized carbon cloth at a current density of 0.1 C; (d) rate capability of doped RM-S/G composite at different current densities.**

hand-milled composite. The increased discharge capacity and capacity retention are due to the better exfoliation and adhesion of graphene in the sulfur particles, which not only increases the active material utilization but also reduces the shuttle phenomenon. In addition, the RM-S/G composite shows excellent Coulombic efficiency of more than 99%.

The RM-S/G composite also shows superior rate performance (Figure 4d), and even at the higher current density of 3 C (5.025 A/g), the RM-S/G composite cathode can still deliver 250 mAh/g of discharge capacity. It has been calculated that, to surpass the current Li-ion technology, it is necessary to load more than 4 mg/$cm^2$ of active material in a cathode.[38] With the conventional aluminum (Al) foil current collector, it is hard to load such a large amount of sulfur because the large volume changes of S/C composite will easily delaminate the thick S/C coating film on Al. A 3-D interconnected conductive network such as carbon cloth has a large accessible surface area with high electrical conductivity and can accommodate and utilize high amounts of active material. Recent reports[39−41] demonstrated that a 3-D network-structured carbon-cloth current collector can load larger amounts of active material while maintaining higher electrical conductivity, thermal stability, and structural integrity. The present 3-D interconnected carbon cloth for sulfur cathode is only used to physically block the high-order polysulfides, however, while maintaining the transport of electrons and ions during charging and discharging of the battery. Recently, Yuan *et al.*[42] reported that heteroatom-doped (boron and nitrogen) carbon powders can enhance the cycling performance and stability of the Li/S system by minimizing the polysulfide shuttle phenomenon. Here, to increase the active material content as well as improve the cycling performance, we have introduced boron, nitrogen-doped carbon cloth as the current collector and active material host.

Figure S4a shows the morphology of the RM-S/G composite-loaded B,N-doped carbon cloth, and Figure S4b shows the energy-dispersive spectroscopy (EDS) mapping of B,N-doped carbon cloth, which confirms the presence of boron and nitrogen in the carbon cloth. The boron and nitrogen come from the tetrafluoroborate anion and the 1-ethyl-3-methylimidazolium cation, respectively. Figure S4a also shows the interaction between the RM-S/G composite and the carbon cloth, which firmly adhere to each other and compose a stable 3-D interconnected network. It is expected that this RM-S/G composite loaded on boron, nitrogen-doped carbon cloth will



DOI: 10.1021/acsnano.7b03591
*ACS Nano* 2017, 11, 9048−9056

show better electrochemical performance along with high active material loading.

Figure 5 shows the electrochemical performance of the RM-S/G-composite-loaded B,N-doped carbon cloth cathode, where each cathode contains more than 8 mg of active materials (~8–9 mg/cm$^2$). The CV curves in Figure 5a show two well-known reduction peaks and one oxidation peak. In the first cycle in Figure 5a, a big shoulder is observed on the oxidation peak, which is due to the lack of contact of the active materials with the electrolyte, which slows the oxidation process, giving rise to a broad shoulder in the oxidation curve rather than a sharp peak. After the first cycle, the electrolyte may have sufficient contact with the sulfur particles, which facilitates oxidation process, and for this reason, the broad shoulder disappears. It is also important to mention here that a similar phenomenon is not observed in Figure 4a, where a low amount of active materials (1–2 mg/cm$^2$) was used in each electrode compared to Figure 5a, where around 8–9 mg/cm$^2$ active materials were used. The low amount of active materials certainly reacts and quickly establishes contact with the electrolyte, so no broad shoulder was observed in Figure 4a. The corresponding two discharge plateaus and one charge plateau were observed in the galvanostatic discharge–charge curves. Both the anodic and the cathodic current increased significantly compared to that in Figure 4a, which confirms the high loading of active materials and their utilization. The cycling performance in Figure 5c shows that, even at the higher loading of 9 mg/cm$^2$, a specific discharge capacity of 1256 mAh/g was still maintained after 200 cycles at a current density of 0.1 C, corresponding to 99% capacity retention of the second cycle capacity. It is important to mention here that there is fluctuation in capacity with cycle numbers. The usage of different amounts of active materials, as well as the polysulfide confinement by the lone pair electrons of boron and nitrogen, may responsible for this phenomenon. In every cycle, there may be some differences in usage of active materials and polysulfide confinement that result in fluctuation in discharge capacity. In sharp contrast, the hand-milled sulfur/graphene composite cathode loaded in B,N-doped carbon cloth exhibits a quick capacity decay to 300 mAh/g after 100 cycles, with capacity retention of 40% at 0.1 C current density due to the high sulfur loading. It can be deduced from the cycling performance that the doped 3-D carbon cloth and the reverse microemulsion method make a significant contribution to achieving higher capacity and better capacity retention. The rate performance of the RM-S/G-composite-loaded, B,N-doped carbon cloth cathode (Figure 5d) also shows that, even at higher current density, this cathode can deliver acceptable discharge capacity and can regain its capacity when low current density is restored.

For sulfur cathode with high active material content (generally more than 5 mg/cm$^2$), precipitation of the sulfur-active material from the current collector is observed due to loss of contact between the current collector and the active material. This sulfur is eventually deposited on the Li anode, which increases the internal impedance of the cell.[43] To analyze this, electrochemical impedance spectroscopy (EIS) was used to measure the evolution of impedance during charge/discharge cycling. Figure S5 shows EIS curves of RM-S/G composite-loaded B,N-doped carbon cloth cathode in the discharged state. The EIS curves show a depressed semicircle followed by an inclined straight line, which reflect the charge transfer resistance and lithium ion diffusion, respectively. It can be seen from the EIS curves that the impedance remains stable over 100 cycles, which indicates that the precipitation of active materials into the electrolyte was effectively suppressed, with the active materials maintaining firm adhesion to the carbon cloth.

## CONCLUSION

Microsized carboxylated graphene/sulfur particles formed by aggregation of primary nano-S/graphene particles were synthesized using a reverse microemulsion method, and the resultant carboxylated graphene sheets could effectively absorb both the sulfur and high-order polysulfides. This synthesized RM-S/G composite showed a very high initial discharge capacity of 914 mAh/g (based on sulfur) and retained discharge capacity of 731 mAh/g after 200 cycles. The electrochemical performance of the RM-S/G composite was further enhanced by using B,N-doped 3-D carbon cloth as a current collector. The RM-S/G composite provided capacity of 1256 mAh/g after 200 cycles, with a capacity decay rate of 0.0127% per cycle at a current density of 0.1 C, even at 8 mg/cm$^2$ of active material loading. This represents one of the best performances among all reported S/G composites at similar sulfur loadings.

## EXPERIMENTAL SECTION

**Preparation of Carboxylated Graphene/Sodium Polysulfide Solution.** Commercial sulfur (6.4 g) was added into 50 mL of 2 M $Na_2S$ aqueous solution. Then, the solution was stirred for several hours until all the sulfur reacted with the $Na_2S$ to form $Na_2S_x$.There was some unreacted sulfur residue powder in the solution, which was filtered out to obtain a clear red $Na_2S_x$ solution. Next, 100 g of carboxylated graphene was added into this solution, and it was sonicated for 10 min to form a homogeneously dispersed graphene/polysulfide solution. All the chemicals, the sulfur, the $Na_2S$, and the carboxylated graphene were purchased from Sigma-Aldrich. The following chemical reaction (reaction 1) occurred for the formation of polysulfides.

$$(x-1)S_8 + 8Na_2S \rightarrow 8Na_2S_x \quad (1)$$

**Preparation of Microemulsions and Graphene/Sulfur Composite.** Thirty grams of a mixture of sorbitan mono-oleate (Span 80) and polyethylene glycol (PEG-20) sorbitan monooleate (Tween 80) in a ratio of 8:1, along with 10 mL *n*-butanol, was added into 450 mL of sulfur-saturated cyclohexane. Both Span 80 and Tween 80 act as surfactants, whereas *n*-butanol and cyclohexane act as a cosurfactant and the oil, respectively. Then, the mixture was homogenized by a Sonic Ruptor-400 ultrasonic homogenizer for 1 h. The homogenized mixture was equally divided into two beakers to prepare two reverse microemulsion solutions. In the first beaker, 12.5 mL of carboxylated graphene-containing $Na_2S_x$ was poured in, and the microemulsion was sonicated again for 10 to 15 min, whereas in the second beaker, 12.5 mL of 4 M HCl was added, and this microemulsion was also sonicated for 10 to 15 min. Finally, these two reverse microemulsions were mixed together and stirred for 2 to 3 h to form the graphene/sulfur composite. The following reaction (reaction 2) occurred when the sulfur precipitated out and formed the graphene/sulfur composite.

$$8Na_2S_x + 16HCl \rightarrow 16NaCl + 8H_2S + (x-1)S_8\downarrow \quad (2)$$

The composite was then separated by centrifugation at 5000 rpm and repeatedly washed with acetone and water to remove all the oils and salts. A schematic illustration of this method is shown in Figure 1, and Figure S1 in the Supporting Information shows the photographs of the different steps. All the chemicals in this case were also purchased from Sigma and directly used without any purification.

**Fabrication of Boron- and Nitrogen-Doped Carbon Cloth.** For the synthesis of boron- and nitrogen-doped carbon cloth, we followed Yuan's method for preparing boron, nitrogen-doped graphene.[42] To do so, small diameter (5 mm) carbon cloth discs were cut and submerged in 1-ethyl-3-methylimidazolium tetrafluoroborate ([Emim]$BF_4$) ionic liquid in an argon-filled glovebox. Then,



DOI: 10.1021/acsnano.7b03591
ACS Nano 2017, 11, 9048–9056

the fully soaked carbon cloths were put into a quartz boat and transferred into a furnace for heat treatment at 330 °C under vacuum. After the heat treatment, the carbon cloths were further annealed at 400 °C in argon to form boron- and nitrogen-doped carbon cloth.

**Fabrication of Electrodes and Coin Cells.** The aluminum current-collector-based cathode was fabricated by using the carboxylated graphene−sulfur precipitated composite, carbon black, and PVDF. The PVDF was added in the amount of 10 wt %, and the amount of carbon black was dependent on the amount of sulfur, which was maintained at 50 wt % of the total amount. The composite, carbon black, and PVDF mixture was manually mixed for 20 to 30 min with the addition of an appropriate amount of *N*-methyl-2-pyrrolidone. The obtained slurry was coated on Al foil to a thickness of 90 $\mu$m and was then dried at 50 °C for 24 h under vacuum. Then, the electrode was cut into 10 mm diameter discs. Each 10 mm disc contained around 1 mg of active materials (sulfur). The fabricated disc electrodes were dried again at 50 °C for a few hours before use. For the carbon-cloth current-collector-based cathode, the slurry was prepared with the addition of carbon black and PVDF, where the sulfur content was 80 wt % along with 10 wt % PVDF and 10 wt % graphene and carbon black. Five millimeter diameter carbon cloth discs were dipped into the slurry and dried in a vacuum oven for 24 h at 50 °C. Each 5 mm diameter carbon cloth disc contained 7.5 to 8.5 mg of sulfur. These discs were then directly used as cathode in the coin cells. The CR 2032 coin-type cells were assembled in an Ar-filled glovebox, where discs of Li foil were used as the counter electrode and reference electrode. The electrolyte was prepared by dissolving 1 M lithium bis-(trifluoromethane sulfonyl)imide and 0.1 wt % $LiNO_3$ in cosolvents of 1,3-dioxolane and 1,2-dimethoxyethane, in a volume ratio of 1:1. A porous polypropylene film was used as the separator.

**Characterization.** To characterize the sulfur−graphene composite and Li−S cells, different analytical tools were used. For physical characterization of the composite, we conducted XRD (Bruker Smart-1000, Bruker AXS Inc., USA) using Cu K$\alpha$ radiation, Raman spectroscopy (Horiba Jobin Yvon Labram Aramis using a 532 nm diode-pumped solid-state laser), FTIR spectroscopy (NEXUS 670 FTIR), TGA (Netzsch STA 449F3, Germany, in an argon environment with a heating rate of 5 °C/min), and four-probe conductivity measurements (Signatone SP4). For morphological analysis, SEM and TEM were conducted on a Hitachi SU-70 analytical SEM (Japan) and a JEOL (Japan) 2100F field emission TEM, respectively. The scanning electron microscope was also used for conducting large-area EDS mapping. For electrochemical performance evaluation of the Li−S cell, an automatic battery tester system (Land, China) was used at various current densities at room temperature within a conventional voltage window (1.5−3 V). EIS and cyclic voltammetry measurements were performed on a Gamry Reference 3000 potentiostat/galvanostat/ZRA with a scan rate of 0.1 mV $s^{-1}$ (within a voltage window of 1.5 to 3 V), and for impedance analysis, a frequency range of 10 mHz to 100 kHz was applied.

## ASSOCIATED CONTENT

### Supporting Information

The Supporting Information is available free of charge on the ACS Publications website at DOI: 10.1021/acsnano.7b03591.

Figures S1−S4 (PDF)

## AUTHOR INFORMATION


### Corresponding Author

*Tel: 301-405-0352. Fax: 301-405-0523. E-mail: cswang@umd.edu.

### ORCID

Mohammad Rejaul Kaiser: 0000-0002-2136-5696

Chunsheng Wang: 0000-0002-8626-6381


### Author Contributions

C.W. designed this work and the experiments; M.R.K. prepared the electrodes and cells, conducted the tests, and wrote the manuscript, and all other authors revised and polished the manuscript.

### Notes

The authors declare no competing financial interest.

## ACKNOWLEDGMENTS

This research has been conducted with the support of the Australian Government Research Training Program Scholarship. In addition, the authors gratefully acknowledge the financial support provided by the Excellerate Australia Professional Development Fund (Grant No. AA2020CRC), an Australian Research Council (ARC) Discovery project (DP1601012627), and support from the Institute for Superconducting and Electronic Materials (ISEM), University of Wollongong, Australia, as well as Nanostructures for Electrical Energy Storage (NEES), an Energy Frontier Research Centre funded by the U.S. Department of Energy, Office of Science, Office of Basic Energy Sciences under Award No. DESC0001160. C.W. acknowledges Heilongjiang Province Natural Science Foundation (key project) (ZD2016-001) and Jiamusi University Technology Innovation Team (Cxtdpy-2016-01) for partial support this work. The authors also thank T. Silver for critical reading of the manuscript.

## REFERENCES


(1) Gur, I.; Sawyer, K.; Prasher, R. Searching for a Better Thermal Battery. *Science* **2012**, *335*, 1454−1455.

(2) Bruce, P. G.; Freunberger, S. A.; Hardwick, L. J.; Tarascon, J.-M. Li-$O_2$ And Li-S Batteries with High Energy Storage. *Nat. Mater.* **2011**, *11*, 19−29.

(3) Ji, X.; Lee, K. T.; Nazar, L. F. A Highly Ordered Nanostructured Carbon-Sulphur Cathode for Lithium-Sulphur Batteries. *Nat. Mater.* **2009**, *8*, 500−506.

(4) Kaiser, M. R.; Wang, J.; Liang, X.; Liu, H.-K.; Dou, S.-X. A Systematic Approach To High and Stable Discharge Capacity for Scaling up The Lithium−Sulfur Battery. *J. Power Sources* **2015**, *279*, 231−237.

(5) Liang, X.; Zhang, M.; Kaiser, M. R.; Gao, X.; Konstantinov, K.; Tandiono, R.; Wang, Z.; Liu, H.-K.; Dou, S.-X.; Wang, J. Split-Half-Tubular Polypyrrole@Sulfur@Polypyrrole Composite with a Novel Three-Layer-3D Structure as Cathode for Lithium/Sulfur Batteries. *Nano Energy* **2015**, *11*, 587−599.

(6) Takahashi, T.; Yamagata, M.; Ishikawa, M. A Sulfur−Microporous Carbon Composite Positive Electrode for Lithium/Sulfur and Silicon/Sulfur Rechargeble Batteries. *Prog. Nat. Sci.* **2015**, *25*, 612−621.

(7) Kaiser, M. R.; Liang, X.; Konstantinov, K.; Liu, H.-K.; Dou, S.-X.; Wang, J.-Z. A Facile Synthesis of High-Surface-Area Sulfur−Carbon Composites for Li/S Batteries. *Chem. - Eur. J.* **2015**, *21*, 10061−10069.

(8) Kaiser, M. R.; Liang, X.; Liu, H.-K.; Dou, S.-X.; Wang, J.-Z. A Methodical Approach for Fabrication of Binder-Free $Li_2S$-C Composite Cathode with High Loading of Active Material for Li-S Battery. *Carbon* **2016**, *103*, 163−171.

(9) Barghamadi, M.; Best, A. S.; Bhatt, A. I.; Hollenkamp, A. F.; Musameh, M.; Rees, R. J.; Ruther, T. Lithium-Sulfur Batteries-The Solution is in The Electrolyte, but is The Electrolyte A Solution? *Energy Environ. Sci.* **2014**, *7*, 3902−3920.

(10) Azimi, N.; Xue, Z.; Rago, N. D.; Takoudis, C.; Gordin, M. L.; Song, J.; Wang, D.; Zhang, Z. Fluorinated Electrolytes for Li-S Battery: Suppressing the Self-Discharge with an Electrolyte Containing Fluoroether Solvent. *J. Electrochem. Soc.* **2015**, *162*, A64−A68.

(11) Hagen, M.; Dörfler, S.; Fanz, P.; Berger, T.; Speck, R.; Tübke, J.; Althues, H.; Hoffmann, M. J.; Scherr, C.; Kaskel, S. Development and Costs Calculation of Lithium−Sulfur Cells with High Sulfur Load and Binder Free Electrodes. *J. Power Sources* **2013**, *224*, 260−268.




DOI: 10.1021/acsnano.7b03591
*ACS Nano* 2017, 11, 9048−9056

(12) Jeddi, K.; Sarikhani, K.; Qazvini, N. T.; Chen, P. Stabilizing Lithium/Sulfur Batteries by a Composite Polymer Electrolyte Containing Mesoporous Silica Particles. *J. Power Sources* **2014**, *245*, 656−662.
(13) Song, M.-K.; Zhang, Y.; Cairns, E. J. A Long-Life, High-Rate Lithium/Sulfur Cell: A Multifaceted Approach to Enhancing Cell Performance. *Nano Lett.* **2013**, *13*, 5891−5899.
(14) Li, G.-C.; Li, G.-R.; Ye, S.-H.; Gao, X.-P. A Polyaniline-Coated Sulfur/Carbon Composite with an Enhanced High-Rate Capability as a Cathode Material for Lithium/Sulfur Batteries. *Advanced Energy Materials.* **2012**, *2*, 1238−1245.
(15) Wang, J.; Chew, S. Y.; Zhao, Z. W.; Ashraf, S.; Wexler, D.; Chen, J.; Ng, S. H.; Chou, S. L.; Liu, H. K. Sulfur-Mesoporous Carbon Composites in Conjunction with A Novel Ionic Liquid Electrolyte for Lithium Rechargeable Batteries. *Carbon* **2008**, *46*, 229−235.
(16) Wang, J. Z.; Lu, L.; Choucair, M.; Stride, J. A.; Xu, X.; Liu, H. K. Sulfur-Graphene Composite for Rechargeable Lithium Batteries. *J. Power Sources* **2011**, *196*, 7030−7034.
(17) Wang, J.; Chen, J.; Konstantinov, K.; Zhao, L.; Ng, S. H.; Wang, G. X.; Guo, Z. P.; Liu, H. K. Sulphur-Polypyrrole Composite Positive Electrode Materials for Rechargeable Lithium Batteries. *Electrochim. Acta* **2006**, *51*, 4634−4638.
(18) Chen, R.; Zhao, T.; Lu, J.; Wu, F.; Li, L.; Chen, J.; Tan, G.; Ye, Y.; Amine, K. Graphene-Based Three-Dimensional Hierarchical Sandwich-type Architecture for High-Performance Li/S Batteries. *Nano Lett.* **2013**, *13*, 4642−4649.
(19) Lu, S.; Cheng, Y.; Wu, X.; Liu, J. Significantly Improved Long-Cycle Stability in High-Rate Li−S Batteries Enabled by Coaxial Graphene Wrapping over Sulfur-Coated Carbon Nanofibers. *Nano Lett.* **2013**, *13*, 2485−2489.
(20) Zhou, G.; Yin, L.-C.; Wang, D.-W.; Li, L.; Pei, S.; Gentle, I. R.; Li, F.; Cheng, H.-M. Fibrous Hybrid of Graphene and Sulfur Nanocrystals for High-Performance Lithium−Sulfur Batteries. *ACS Nano* **2013**, *7*, 5367−5375.
(21) Lin, T.; Tang, Y.; Wang, Y.; Bi, H.; Liu, Z.; Huang, F.; Xie, X.; Jiang, M. Scotch-Tape-Like Exfoliation of Graphite Assisted With Elemental Sulfur and Graphene-Sulfur Composites for High-Performance Lithium-Sulfur Batteries. *Energy Environ. Sci.* **2013**, *6*, 1283−1290.
(22) Xu, C.; Xu, B.; Gu, Y.; Xiong, Z.; Sun, J.; Zhao, X. S. Graphene-Based Electrodes for Electrochemical Energy Storage. *Energy Environ. Sci.* **2013**, *6*, 1388−1414.
(23) Bagwe, R. P.; Yang, C.; Hilliard, L. R.; Tan, W. Optimization of Dye-Doped Silica Nanoparticles Prepared Using a Reverse Microemulsion Method. *Langmuir* **2004**, *20*, 8336−8342.
(24) Capek, I. Preparation of Metal Nanoparticles in Water-In-Oil (W/O) Microemulsions. *Adv. Colloid Interface Sci.* **2004**, *110*, 49−74.
(25) Yang, Y.; Gao, M. Y. Preparation of Fluorescent $SiO_2$ Particles with Single CdTe Nanocrystal Cores by the Reverse Microemulsion Method. *Adv. Mater.* **2005**, *17*, 2354−2357.
(26) Koole, R.; van Schooneveld, M. M.; Hilhorst, J.; de Mello Donegá, C.; Hart, D. C.; van Blaaderen, A.; Vanmaekelbergh, D.; Meijerink, A. On the Incorporation Mechanism of Hydrophobic Quantum Dots in Silica Spheres by a Reverse Microemulsion Method. *Chem. Mater.* **2008**, *20*, 2503−2512.
(27) Gibaud, S.; Attivi, D. Microemulsions for Oral Administration and Their Therapeutic Applications. *Expert Opin. Drug Delivery* **2012**, *9*, 937−951.
(28) Lagourette, B.; Peyrelasse, J.; Boned, C.; Clausse, M. Percolative Conduction in Microemulsion Type Systems. *Nature* **1979**, *281*, 60−62.
(29) Meyer, B. Elemental Sulfur. *Chem. Rev.* **1976**, *76*, 367−388.
(30) Davies, R.; Graham, D. E.; Vincent, B. Water-Cyclohexane-"Span 80"-"Tween 80" Systems: Solution Properties and Water/Oil Emulsion Formation. *J. Colloid Interface Sci.* **1987**, *116*, 88−99.
(31) Kunieda, H.; Ishikawa, N. Evaluation of The Hydrophile-Lipophile Balance (HLB) of Nonionic Surfactants. II. Commercial-Surfactant Systems. *J. Colloid Interface Sci.* **1985**, *107*, 122−128.
(32) Harvey, P. D.; Butler, I. S. Raman Spectra of Orthorhombic Sulfur at 40 K. *J. Raman Spectrosc.* **1986**, *17*, 329−334.
(33) Sadezky, A.; Muckenhuber, H.; Grothe, H.; Niessner, R.; Pöschl, U. Raman Microspectroscopy of Soot and Related Carbonaceous Materials: Spectral Analysis and Structural Information. *Carbon* **2005**, *43*, 1731−1742.
(34) Liang, X.; Wen, Z.; Liu, Y.; Zhang, H.; Huang, L.; Jin, J. Highly Dispersed Sulfur in Ordered Mesoporous Carbon Sphere as a Composite Cathode for Rechargeable Polymer Li/S Battery. *J. Power Sources* **2011**, *196*, 3655−3658.
(35) Zu, C.; Klein, M.; Manthiram, A. Activated $Li_2S$ as a High-Performance Cathode for Rechargeable Lithium−Sulfur Batteries. *J. Phys. Chem. Lett.* **2014**, *5*, 3986−3991.
(36) Meini, S.; Elazari, R.; Rosenman, A.; Garsuch, A.; Aurbach, D. The Use of Redox Mediators for Enhancing Utilization of $Li_2S$ Cathodes for Advanced Li-S Battery Systems. *J. Phys. Chem. Lett.* **2014**, *5*, 915−918.
(37) Zhang, S. S. Effect of Discharge Cutoff Voltage on Reversibility of Lithium/Sulfur Batteries with $LiNO_3$-Contained Electrolyte. *J. Electrochem. Soc.* **2012**, *159*, A920−A923.
(38) Manthiram, A.; Fu, Y.; Su, Y.-S. Challenges and Prospects of Lithium−Sulfur Batteries. *Acc. Chem. Res.* **2013**, *46*, 1125−1134.
(39) Dang, L.; Wei, C.; Ma, H.; Lu, Q.; Gao, F. Three-Dimensional Honeycomb-Like Networks of Birnessite Manganese Oxide Assembled by Ultrathin Two-Dimensional Nanosheets With Enhanced Li-Ion Battery Performances. *Nanoscale* **2015**, *7*, 8101−8109.
(40) Mao, S.; Lu, G.; Chen, J. Three-Dimensional Graphene-Based Composites for Energy Applications. *Nanoscale* **2015**, *7*, 6924−6943.
(41) Lingappan, N.; Van, N. H.; Lee, S.; Kang, D. J. Growth Of Three Dimensional Flower-Like Molybdenum Disulfide Hierarchical Structures on Graphene/Carbon Nanotube Network: An Advanced Heterostructure for Energy Storage Devices. *J. Power Sources* **2015**, *280*, 39−46.
(42) Yuan, S.; Bao, J. L.; Wang, L.; Xia, Y.; Truhlar, D. G.; Wang, Y. Graphene-Supported Nitrogen and Boron Rich Carbon Layer for Improved Performance of Lithium−Sulfur Batteries Due to Enhanced Chemisorption of Lithium Polysulfides. *Advanced Energy Materials.* **2016**, *6*, 1501733.
(43) Qie, L.; Manthiram, A. A Facile Layer-by-Layer Approach for High-Areal-Capacity Sulfur Cathodes. *Adv. Mater.* **2015**, *27*, 1694−1700.


DOI: 10.1021/acsnano.7b03591
*ACS Nano* 2017, 11, 9048−9056